INTERNATIONAL JOURNAL OF CLIMATOLOGY
Int. J. Climatol. **31**: 1074–1087 (2011)
Published online 14 April 2011 in Wiley Online Library
(wileyonlinelibrary.com) DOI: 10.1002/joc.2336

RMetS
Royal Meteorological Society

El Niño/Southern Oscillation behaviour since 1871 as diagnosed in an extended multivariate ENSO index (MEI.ext)

Klaus Wolter[a]* and Michael S. Timlin[b]

[a] *University of Colorado-CIRES Climate Diagnostics Center and NOAA-ESRL Physical Science Division, Boulder, Colorado, R/PSD1 325 Broadway, Boulder, CO 80305-3328. USA*

[b] *Midwestern Regional Climate Center, CAS/ISWS/INRS, University of Illinois, Champaign, Illinois, USA*

ABSTRACT: El Niño/Southern Oscillation (ENSO) remains the most important coupled ocean–atmosphere phenomenon to cause global climate variability on seasonal to interannual time scales. This paper addresses the need for a reliable ENSO index that allows for the historical definition of ENSO events in the instrumental record back to 1871. The Multivariate ENSO Index (MEI) was originally defined as the first seasonally varying principal component of six atmosphere–ocean (COADS) variable fields in the tropical Pacific basin. It provides for a more complete and flexible description of the ENSO phenomenon than single variable ENSO indices such as the SOI or Niño 3.4 SST. Here we describe our effort to boil the MEI concept down to its most essential components (based on SLP, SST) to enable historical analyses that more than double its period of record to 1871–2005. The new MEI.ext confirms that ENSO activity went through a lull in the early- to mid-20th century, but was just about as prevalent one century ago as in recent decades. We diagnose strong relationships between peak amplitudes of ENSO events and their duration, as well as between their peak amplitudes and their spacing (periodicity). Our effort is designed to help with the assessment of ENSO conditions through as long a record as possible to be able to differentiate between 'natural' ENSO behaviour in all its rich facets, and the 'Brave New World' of this phenomenon under evolving GHG-related climate conditions. So far, none of the behaviour of recent ENSO events appears unprecedented, including duration, onset timing, and spacing in the last few decades compared to a full century before then. Copyright © 2011 Royal Meteorological Society

KEY WORDS history; ENSO; MEI

Received 30 July 2009; Revised 24 September 2010; Accepted 4 March 2011

1. Introduction

While Sir Gilbert Walker will forever be associated with his research on the 'Southern Oscillation' (SO; Walker and Bliss, 1932), several other researchers noticed this pressure seesaw before him around the turn of the 20th century (e.g. Philander, 1991, p.9). Nevertheless, the description of the SO in Walker and Bliss (1932) is of interest here since it remains the paper that clearly defined the SO as a multivariate phenomenon, using near-surface air temperature, rainfall, as well as sea level pressure (SLP) rather than just the latter. In addition, Walker and Bliss considered the SO separately for the two seasons, Dec–Feb and Jun–Aug, noting that '... conditions are related differently in winter and summer'. In both aspects, using more than one observational field, and differentiating by seasons, the Multivariate ENSO index (MEI; Wolter and Timlin, 1993, 1998) came full circle after a long series of ENSO indices that had been based on single variable fields, and that had not been allowed to vary with the seasonal cycle. Ruling supreme until the 1980s, the Southern Oscillation Index (SOI) was defined by Troup (1965) as the normalized SLP difference between Tahiti and Darwin, and was extended several times by Jones and collaborators (Allan *et al*., 1991). Once the link between the SO and El Niño was established (Bjerknes, 1966, 1969), Rasmusson and Carpenter (1982) described so-called Niño regions (1, 2, 3, and 4) based on ship-tracks, but it was only just over a decade ago that Barnston *et al*. (1997) defined the so-called Niño 3.4 SST region that maximizes the ENSO signal among SST-based indices, thus launching the most popular ENSO index of the last decade.

Meanwhile, different portions of Walker's SO index were rediscovered and extended by Peter Wright, first with combinations of SLP stations (Wright, 1975), then with a rainfall station index for the Central Pacific and with a so-called Cold Tongue SST index (CTI) that summarizes equatorial SST anomalies from the dateline to the South American coast (Wright, 1984, 1989). While he never combined different fields into a single unified index, he used all three to diagnose

* Correspondence to: Klaus Wolter, University of Colorado-CIRES Climate Diagnostics Center and NOAA-ESRL Physical Science Division, Boulder, Colorado, R/PSD1 325 Broadway, Boulder, CO 80305-3328. USA. E-mail: Klaus.Wolter@noaa.gov

ENSO events. At least one version of the CTI is kept up to date at the University of Washington (website: http://www.jisao.washington.edu/data/cti/), but we are not aware of a similar product for Wright's rainfall index. Working initially with tropical ship data for the Indian and Atlantic Oceans, as well as the easternmost Pacific, Wolter (1989) determined that ENSO is the most prominent global tropical circulation mode even outside the Pacific basin, leading eventually to the definition of the Multivariate ENSO Index (MEI) as the first principal component of six observed fields (SLP, zonal and meridional surface wind components, SST, near-surface air temperatures, and total cloudiness; Wolter and Timlin, 1993, 1998), using the Comprehensive Ocean-Atmosphere Data Set (COADS; Worley *et al*., 2005) for the original MEI base period from 1950–1993.

Since the MEI was introduced to the Web (online since 1997: http://www.noaa.esrl.noaa.gov/psd/people/klaus.wolter/MEI/), others have (re) discovered the concept of using more than one variable to monitor ENSO. For instance, Smith and Sardeshmukh (2000) joined the SOI and Niño 3.4 SST anomalies into a 'Bivariate ENSO Timeseries' (BEST) index in the simplest possible fashion. Allan (2000) combined SST and SLP fields through joint EOF-analyses, but the resulting indices were split into different spectral bands, and were apparently never intended for near-realtime monitoring. After more than a decade of monthly Web updates of the MEI, we have recently begun to explore (1) how robust the MEI is with respect to a variety of changes in its computation and composition, (2) how the utility of the MEI can be evaluated compared to other ENSO indices, and (3) how far back in time the MEI concept can be extended. While the first two issues will be addressed elsewhere, the paper at hand examines the last issue.

We had earlier investigated pre-1950 versions of the MEI in COADS, but found that wind fields in particular had severe problems with respect to changes in measurement techniques, including the shift from sail to motorized ships in the late 19th century, and from sea-state estimates to anemometer measurements in the middle of the 20th century (Ramage, 1987). While reliable homogenized surface wind data appear to be elusive thus far, there have been several successful efforts to create instrumental bias-corrected SST and SLP grids (in particular, Kaplan *et al*., 1998; Smith and Reynolds, 2003; and Rayner *et al*., 2003, for the former, and Allan and Ansell, 2006, for the latter) that push the instrumental record back well into the 19th century. In the context of exploring the overall MEI approach, we felt the time was ripe to investigate a simplified version of the MEI that is based on reconstructed SLP and SST fields as far back as possible. This paper documents this effort to create an extended MEI (in the following called MEI.ext) for the period 1871–2005 (Section 2), makes some basic comparisons with other established ENSO indices (Section 3), establishes its basic spatial and temporal features, and examines ENSO behaviour over the full record (Section 4). A discussion and concluding remarks wrap up this paper in Section 5.

2. Data and construction of extended MEI (MEI.ext)

While this paper is mostly about the MEI.ext, we acknowledge the need to relate it to other ENSO indices. With regard to the SOI, we downloaded three different versions, one from the Climate Research Unit (CRU) at the University of East Anglia in England (http://www.cru.uea.ac.uk/cru/data/soi.htm based on Allan *et al*., 1991), one from the Bureau of Meteorology (BMRC) in Australia (http://www.bom.gov.au/climate/current//soihtm1.shtml based on Troup, 1965), and one from the US Climate Prediction Center (CPC) in Washington, DC (metadata: http://www.cpc.ncep.noaa.gov/data/indices/Readme.index.shtml#SOICALC; data: http://www.cpc.ncep.noaa.gov/data/indices/soi). They are all based on SLP data from Tahiti (17° 32′S, 149° 34′W) and Darwin (12° 27′S, 130° 50′W). Tropical Pacific SST fields (including time series for the Niño 3.4 region: 5 °N–5 °S, and 120°–170 °W) were computed from three different reconstructions: HadSST2 (Rayner *et al*., 2006), Kaplan (Kaplan *et al*., 1998), and ERSST (Version 2; Smith *et al*., 2004). Tropical Pacific SLP fields were based on HadSLP2 data (Allan and Ansell, 2006). We also included the following ENSO indices in our analysis: the 'Cold Tongue Index' (CTI; http://www.jisao.washington.edu/data/cti/) that is based on bias-adjusted COADS data; the 'Bivariate ENSO Timeseries' (BEST; based on a standardized SOI and HadSST Niño 3.4 data: http://www.noaa.esrl.noaa.gov/data/climateindices/list/#BEST); and the original MEI (metadata: http://www.noaa.esrl.noaa.gov/psd/people/klaus.wolter/MEI/; data: http://www.noaa.esrl.noaa.gov/psd/people/klaus.wolter/MEI/table.html).

Monthly HadSST2 data commences in 1871 and is provided at 1×1 degree lat $\times$ long resolution, while HadSLP2 is rendered in 5×5 degree resolution, beginning in 1850. Both were converted into 2×2 degree fields, followed by a second conversion into 4×4 degree grids centred on the Equator and starting at the Greenwich Meridian by using the median value of each set of four 2×2 degree boxes to make them compatible with prior MEI analyses based on COADS (Wolter and Timlin, 1993, 1998). In that spirit, the analysis domain was kept the same as for the original MEI: 30 °N–30 °S, and 100 °E–70 °W, excluding the Atlantic Ocean. Area weights were assigned to each 4×4 degree box by multiplying the overall size of each box (which depends on the latitude) by the percentage of ocean coverage within the box. Sliding bimonthly seasonal values were calculated for all 12 possible seasons (December-January 1871–2005, ..., November–December 1871–2005), or 12 times 135 values for each 4×4 degree box. These time series were normalized by computing the bimonthly anomalies from the respective 135-year averages, and

by dividing them by the respective standard deviations in order to focus on the most coherent behaviour rather than on high local variance. The normalized time series were then multiplied with the respective area weights to create input time series for the principal component analysis. This is similar to our original MEI design (Wolter and Timlin, 1993), except that larger areal averages were created through the use of cluster analysis. Given that setup, the largest and most coherent clusters dominated the subsequent principal component analysis (Wolter and Timlin, 1993). While we discarded the clustering step in the computation of MEI.ext, we wanted to keep the rest of its calculation as close as possible to the original MEI blueprint.

Un-rotated principal component Analysis (PCA) was performed on the combined HadSST2 and HadSLP2 fields for each of the aforementioned 12 sliding bimonthly seasons. Since the total area of the analysis domain is the same for both SLP and SST fields, the total variance of either field is equal to the other one. This is a desirable feature that was originally suggested by Lorenz (1956) as the best way to match different fields in a combined PCA-type analysis. We used the covariance matrix for this PCA to preserve the area-weighted relationships between the SST and SLP fields. Wolter (1989) had examined principal component solutions based on correlation as well as covariance matrices of combined fields, and found relatively small differences for the leading eigenvectors.

Analogous to the original MEI (Wolter and Timlin, 1993, 1998), the MEI.ext is defined as the first principal component of the current analysis. In addition to using just two variable fields instead of six, the main difference compared to the original MEI is the omission of the spatial clustering step that we found to be of minor importance in our recent MEI work. While the current MEI.ext was computed using HadSST2 and HadSLP2 data, we also created MEI.ext versions using Kaplan and ERSST data, finding remarkably little difference, in particular between the Kaplan and Hadley Centre versions (all three MEI.ext versions correlate at 0.98 or higher with each other).

In order to reassure the reader that the extended MEI.ext is a fair substitute for the original MEI, Figure 1 shows a scatter plot between these two index time series during 1950–2005, both normalized to this common period of record. There is a well known (An and Jin, 2004) asymmetry of ENSO that allows El Niño events to get more extreme in terms of positive SST anomalies than La Ninã events to the negative side. Confirming this, we computed positive skewness values for all examined ENSO indices in this paper except for the (non-SST based) Jones SOI. In terms of both MEI indices, the positive skewness translates into only a few negative values below −2 since 1950, but positive values of up to +3 and higher. This skewness is the main reason we use non-parametric thresholds (rankings) to define the strength of ENSO events rather than fixed symmetrical thresholds, such as +/−0.5 °C for Niño 3.4 SST anomalies (practice at CPC; Kousky and Higgins, 2007). In Figure 1, the average absolute difference between MEI and MEI.ext is less than 0.2 standard deviations, but reaches one standard deviation or higher on three occasions out of 672 possible bimonthly matches, with two of these during boreal spring when both indices explain the least variance of their component fields. The linear correlation between MEI and MEI.ext is +0.968 for the period 1950–2005 across all seasons, higher than that between either one of them with any other ENSO index. By comparison, the linear correlation between the original MEI and an experimental MEI version that uses COADS instead of Hadley Centre fields of SLP and SST is only slightly higher at +0.977, showing that differences between MEI and MEI.ext are due more to the reduction from six to two variable fields and the omission of clusters than the switch from COADS to Hadley Centre data.

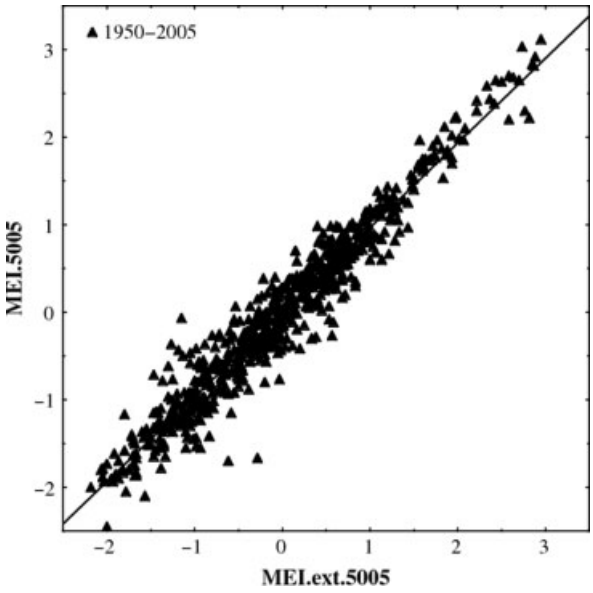

Figure 1. Scatter plot of MEI *versus* MEI.ext time series values, normalized to 1950–2005 means and standard deviations for each of 12 sliding seasons (672 cases); r**2 = 93.7%.

3. Comparison of MEI.ext with other ENSO indices

While the MEI.ext is defined on a sliding bimonthly basis, we also created longer seasonal averages to allow for comparisons with other ENSO indices, in particular, the SOI which is typically averaged across up to five months due to its volatility (Wright, 1989). This smoother MEI.ext version combined three bimonthly seasonal values each to get at the four cardinal seasons: Nov–Dec, Dec–Jan, and Jan–Feb were averaged into the boreal winter season (NDJF), and analogously for the other three seasons. This makes it easier to relate the MEI.ext to seasonal impacts during the conventional meteorological seasons (Dec–Feb, ..., Sep-Nov).

Relationships among a wide variety of ENSO indices are documented in Table I, using four-monthly seasonal values that were constructed in identical fashion for all

Table I(a). Correlation matrix of ENSO indices during 1950–05 using four-month seasons for the 'Cold Tongue Index' (CTI) and HadISST Niño 3.4 SST (HN34), the 'Bivariate ENSO Index' (BEST), Jones and CPC SOI (both sign-reversed), as well as the original MEI and MEI.ext. Lowest correlations are marked in *italics*, while highest correlations are marked in **bold** lettering. Correlations between similar indices (Jones and CPC-SOI, as well as MEI *vs* MEI.ext) are **underlined** and in **bold**

	CTI	HN34.	BEST	Jones	CPC	MEI
HN34. ndjf	**0.964**					
BEST.ndjf	0.938	0.962				
Jones.ndjf	*0.857*	0.873	0.953			
CPC-SOI.ndjf	0.858	0.876	0.962	**0.992**		
MEI.ndjf	0.944	0.964	0.962	0.924	0.921	
MEI.ext.ndjf	0.949	0.970	0.957	0.912	0.909	**0.993**
HN34fmam	0.854					
BEST.fmam	0.855	0.947				
Jones.fmam	0.776	0.856	0.943			
CPC-SOI. Fmam	0.789	0.887	**0.970**	**0.970**		
MEI.fmam	0.839	0.902	0.917	0.877	0.903	
MEI.ext.fmam	0.853	0.968	0.953	0.894	0.921	**0.969**
HN34mjja	0.884					
BEST.mjja	0.884	0.945				
Jones.mjja	*0.721*	0.807	0.931			
CPC-SOI.mjja	0.739	0.825	**0.952**	**0.983**		
MEI.mjja	0.879	0.929	0.907	0.829	0.837	
MEI.ext.mjja	0.882	0.945	0.908	0.823	0.826	**0.969**
HN34.ason	0.943					
BEST.ason	0.924	**0.977**				
Jones.ason	*0.850*	0.892	0.957			
CPC-SOI.ason	0.858	0.903	0.966	**0.966**		
MEI.ason	0.921	0.954	0.962	0.928	0.934	
MEI.ext.ason	0.931	0.963	0.961	0.921	0.927	**0.987**

involved indices. We reversed the sign of both SOIs to have them represent El Niño events with positive numbers. Within the more recent period (1950–2005), Table I(a) shows that most ENSO indices correlate very well with each other during the boreal autumn and winter seasons, with weaker agreement in the other seasons. Specifically, the two SST indices (HN34 and CTI) correlate between 0.85 in boreal spring and 0.96 in boreal winter, while the two SOIs (CPC and Jones) correlate even higher, between 0.97 and 0.99. The BMRC SOI correlates highest with the CPC SOI (above 0.985 for any season; not shown); thus, it was removed as redundant from this table. As discussed with respect to Figure 1, MEI and MEI.ext correlate at just about the same strength with each other as the SOIs, between 0.97 and 0.99 for the four four-monthly seasons, despite considerably larger differences in their construction than for the SOIs.

In terms of comparing across categories of ENSO indices, the 'BEST' index correlates highest with all other ENSO indices, between 0.84 (with Jones SOI in boreal summer) and 0.98 (with HN34 in boreal autumn). Right behind it, both the MEI and MEI.ext correlate at least at 0.83 and 0.82, respectively, with the Jones SOI in boreal summer, and up to 0.96 and 0.97 with HN34 in boreal winter. Both the BEST and MEI indices have the lowest risk of 'missing' any ENSO event that is flagged in any ENSO index, at least since 1950. Since both MEIs are fundamentally different from all other ENSO indices in their construction, one could argue that they capture ENSO features (especially, their seasonality) that are not retrieved by any other index. Therefore, they should not be expected to correlate at the very highest possible level with all other ENSO indices, even though high correlation coefficients are reassuring.

Table I(b). As in Table I(a), except during 1871–1949, for: HN34, BEST, Jones, and MEI.ext

	CTI	HN34	BEST	Jones
HN34ndjf	0.928			
BEST.ndjf	0.889	0.941		
Jones.ndjf	*0.714*	0.739	0.914	
MEI.ext.ndjf	0.904	**0.968**	0.942	0.774
HN34fmam	0.804			
BEST.fmam	0.798	0.927		
Jones.fmam	*0.588*	0.646	0.869	
MEI.ext.fmam	0.789	**0.935**	0.895	0.645
HN34mjja	0.758			
BEST.mjja	0.787	0.843		
Jones.mjja	0.537	*0.460*	0.852	
MEI.ext.mjja	0.780	**0.901**	0.856	0.553
HN34ason	0.893			
BEST.ason	0.844	0.900		
Jones.ason	*0.615*	0.620	0.894	
MEI.ext.ason	0.874	**0.939**	0.912	0.689

For the period of record before 1950, Table I(b) confirms that the (Jones) SOI shows the lowest correlations

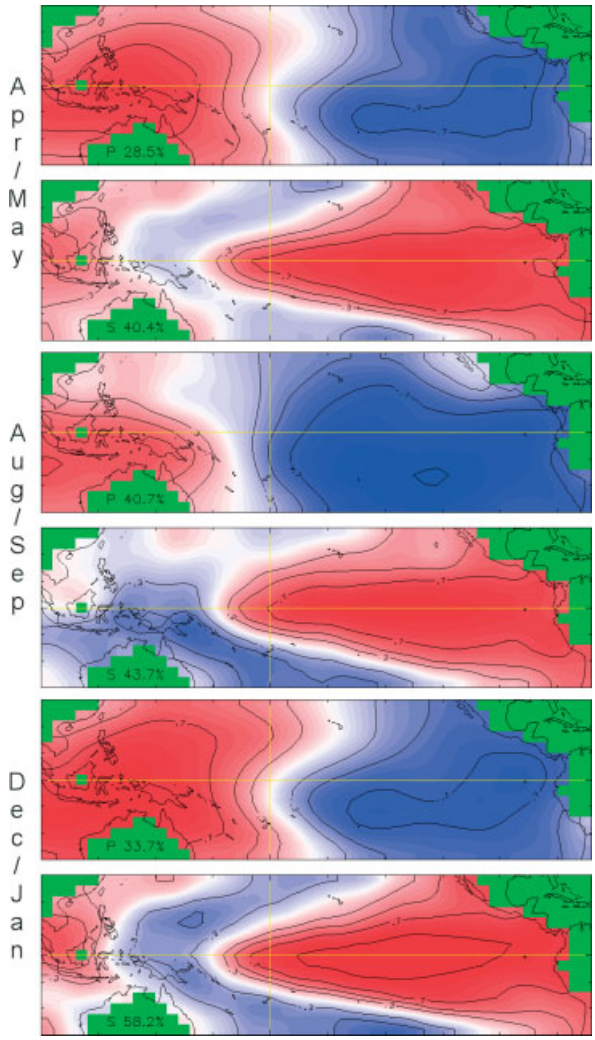

Figure 2. MEI.ext loadings for sea level pressure (P) and sea surface temperatures (S) based on gridded Hadley Centre data for Apr–May (top), Aug–Sep (middle), and Dec–Jan (bottom) during 1871–2005. Both the Equator and dateline are marked in yellow, and there are tick-marks for every 10° latitude as well as 20° longitude.

with all other ENSO indices, especially with pure SST indices such as CTI (lowest in all seasons except for boreal summer) and HN34 (lowest in boreal summer). If one were to use the Australian SOI (which commences in 1876), one would get slightly higher correlation coefficients (not shown). The BEST index maintains its overall highest correlation levels with all other indices, between 0.79 (with Jones SOI in boreal summer) and 0.94 with both HN34 and MEI.ext in boreal winter. Possibly due to the smoothed nature of HadSST, and the fact that the Niño 3.4 region is embedded in the highest loadings for the SST portion of the extended MEI (Figure 2 in Section 4.1), it may not come as a surprise that the highest correlations of the pre-1950 epoch are found between MEI.ext and HN34 in all seasons, even though that correlation still bottoms out at 0.90 in boreal summer. In sum, the MEI.ext appears to describe the same ENSO phenomenon as other ENSO indices, and features similar correlation coefficients with these other ENSO indices as found for the original MEI.

It should be noted that even correlations of +0.90 do not prevent significant differences in rankings. During the best correlated season (boreal winter), *all* five ENSO indices flag 1878, 1983, and 1998 among the top five El Niño rankings since 1871 (Table II documents this for the MEI.ext in the next section). The 2 remaining highest ranking events are shared among 6 years (number of ENSO indices with top 5 listings in parentheses): 1889(3), 1919(1), 1931(1), 1941(1), 1973(2), and 1992(2). The coherency is even weaker for the highest ranked La Niña events, where *none* of the 5 used indices ever agree completely (1974 comes closest with 4 shared top 5 rankings), and a total of *14* years are needed to cover the 5 highest ranked La Niña winters for all 5 indices. Even in boreal winter, the choice of index can thus result in different years when composites are computed for any type of ENSO event, but especially for La Niña, with potentially large differences in these composites.

4. Results

4.1. Spatial features of the MEI.ext

While all other ENSO indices remain fixed in their spatial domain, the MEI allows for geographic variations in its seasonal features. Figure 2 documents the loadings fields for MEI.ext for 3 out of 12 seasons (April–May, August–September, and December–January) during the full period of record (1871–2005). 'Loadings' represent the linear correlation coefficients between time series of gridded local anomalies and MEI.ext. Land areas and Atlantic waters are flagged in green. Each variable is denoted by a single capitalized letter, and shows the explained variance for the same field in the 'Australian corner'. For all seasons, the sea level pressure (P) loadings in Figure 2 reveal the familiar dipole pattern of the SO: high pressure anomalies in the west and low pressure anomalies in the east correspond to positive MEI values, or El Niño-like conditions. Comparing the three seasons, the latitudinal position of the highest loadings ('center of gravity', see Wolter and Timlin, 1993) is furthest north for both poles of the SO during April–May (near the Equator; top panel of Figure 2). This is also furthest away from Tahiti and Darwin, respectively. Four months later (Figure 2, middle panel), the highest loadings have shifted back south towards the classic dipole position of the SO during the season that the total explained SLP variance reaches its peak. In boreal winter (December–January; bottom panel of Figure 2), the MEI.ext explains the most overall variance of both fields combined, and the pressure dipole shows its highest east-west symmetry.

The sea surface temperature field (S) exhibits the typical ENSO signature of a near-equatorial wedge of positive loadings stretching from the Central and

Table II. Four-month seasonal table (NDJF, FMAM, MJJA, ASON) for MEI.ext that goes from 1871 to 2005 and shows which seasons could be classified as **strong/moderate/***weak* El Niño/La Niña events (or neutral). The upper (lower) 10 percentile (ranks 123 and higher/13 and lower) is used for the **strong** El Niño (La Niña) category, upper (lower) 20 percentile for **moderate** cases (ranks 109/27), and upper (lower) 30 percentile for *weak* cases (95/41).

Year	NDJF	FMAM	MJJA	ASON	Year	NDJF	FMAM	MJJA	ASON
1871	63	79	*36*	71	1941	**120**	**131**	**128**	**126**
1872	42	*39*	*34*	*36*	1942	**122**	*108*	*37*	**21.5**
1873	**24**	**12**	*35*	58	1943	**15**	48	86	49
1874	*38*	**15**	**20**	**24**	1944	58	81	76	55
1875	*36*	**21**	**3**	**20**	1945	54	52	52	69
1876	**25**	**4**	**10**	64	1946	62	59	65	87
1877	86	87	**120**	**133**	1947	82	54	54	*37*
1878	**133**	**130**	92	*35*	1948	71	93	75	63
1879	**27**	43	**27**	*38*	1949	70	64	48	*32*
1880	**23**	**23**	70	68	1950	**20**	**10**	**6**	**13**
1881	83	70	56	43	1951	**12**	*40*	*107*	**115**
1882	*41*	*32*	*33*	50	1952	*101*	91	61	76
1883	45	*36*	45	66	1953	81	*107*	91	93
1884	79	89	*95*	94	1954	75	67	*30*	**21.5**
1885	*98*	86	79	*108*	1955	**21**	**11**	**4**	**3**
1886	92	57	**11**	**12**	1956	**3**	**9**	**14.5**	**26**
1887	**9**	**14**	55	65	1957	*37*	88	**126**	**122**
1888	80	**113**	**117**	**130**	1958	**125**	**126**	**124**	92
1889	**130**	**120**	*38*	**9**	1959	*102*	**112**	*102*	79
1890	**6**	**7**	**9**	**18**	1960	72	74	64	53.5
1891	47	76	82	74	1961	69	73	77	51
1892	61	**13**	**19**	**6**	1962	*29*	44	*40*	*40*
1893	**5**	**5**	**1**	**2**	1963	52	58	*100*	**118**
1894	**11**	**8**	**24**	*29*	1964	**109**	53	**18**	**14**
1895	*34*	*33*	62	86	1965	*40*	75	**125**	**127**
1896	65	65	**111**	**123**	1966	**128**	**115**	90	73
1897	**124**	**118**	74	46	1967	57	*41*	*32*	*34*
1898	46	*30*	47	*33*	1968	48	*37*	46	*97*
1899	44	56	*96*	**112**	1969	*108*	**117**	**116**	*106*
1900	**115**	**125**	**121**	91	1970	*103*	82	**21**	**15**
1901	*96*	69	69	47	1971	**10**	**1**	**12**	**11**
1902	55	*97*	**129**	**129**	1972	*39*	80	**133**	**132**
1903	**116**	*96*	*41*	*39*	1973	**132**	**109**	**22**	**7**
1904	**17**	**27**	80	*103*	1974	**1**	**3**	**25**	*31*
1905	*107*	**121**	**131**	**125**	1975	*31*	**25**	**8**	**1**
1906	**114**	92	60	**25**	1976	**4**	**16**	94	**117**
1907	*30*	*28*	44	70	1977	*105*	*99*	*103*	**109**
1908	49	**22**	**23**	**23**	1978	**113**	94	67	77
1909	**22**	*29*	**7**	**8**	1979	*97*	83	*99*	*107*
1910	**8**	**2**	**2**	**10**	1980	**112**	**119**	*108*	88
1911	**19**	**20**	29	*96*	1981	67	77	68	80
1912	**110**	*100*	43	67	1982	77	*95*	**130**	**134**
1913	76	47	72	*98*	1983	**135**	**135**	**132**	81
1914	*106*	*102*	*105*	**119**	1984	73	66	49	59
1915	**118**	**122**	**114**	53.5	1985	*32*	*31*	51	52
1916	43	**24**	**5**	**4**	1986	60	68	93	**120**
1917	**2**	**6**	**14.5**	**16**	1987	**123**	**132**	**134**	**131**
1918	**14**	*35*	**109**	**113**	1988	**121**	85	**13**	**5**
1919	**127**	**123**	**119**	*104*	1989	**7**	**17**	**26**	48
1920	89	*98*	66	62	1990	85	*105*	84	89
1921	74	**26**	*39*	*41*	1991	90	**111**	**113**	*105*

Table II. (*Continued*).

Year	NDJF	FMAM	MJJA	ASON	Year	NDJF	FMAM	MJJA	ASON
1922	50	62	50	44	1992	**129**	**133**	**127**	*100*
1923	*33*	45	89	**111**	1993	**111**	**127**	**122**	**114**
1924	*104*	55	**16**	**17**	1994	*99*	*103*	**110**	**121**
1925	**26**	60	87	**124**	1995	**119**	**114**	*97*	56
1926	**126**	**128**	**112**	75	1996	51	50	57	57
1927	78	61	53	85	1997	53	*101*	**135**	**135**
1928	91	72	78	45	1998	**134**	**134**	81	*30*
1929	66	63	*101*	*101*	1999	**18**	**19**	*28*	**27**
1930	*95*	**116**	**118**	**128**	2000	**13**	**18**	42	61
1931	**131**	**129**	*98*	82	2001	*35*	46	59	60
1932	84	**110**	**115**	78	2002	64	84	*106*	**116**
1933	68	49	*31*	**19**	2003	**117**	*106*	71	*95*
1934	**16**	42	63	72	2004	94	78	88	*102*
1935	59	51	73	90	2005	93	*104*	*104*	42
1936	87	90	85	83					
1937	88	71	58	84					
1938	56	*38*	**17**	*28*					
1939	*28*	*34*	83	*99*					
1940	*100*	**124**	**123**	**110**					

South American coasts to slightly west of the dateline (Figure 2), or warm anomalies during an El Niño event. To the north- and southwest, a horseshoe-like feature of negative loadings indicates the well known tendency for opposite SST anomalies to occur east of Australia and east of the Philippines (Rasmusson and Carpenter, 1982), stretching into the subtropics in both hemispheres. These negative loadings peak northeast of Australia during austral spring (Figure 2, middle panel). Positive loadings are highest during the boreal winter season (Figure 2, bottom panel), and stay along the Equator between the dateline and 100 °W throughout the year, always encompassing the Niño 3.4 region (120°–170 °W, 5 °N–5 °S). The dropoff in loading strength from about Galapagos eastward to South America is most easily seen in boreal winter and spring (bottom and top panels of Figure 2, respectively). This is consistent with the lack of strong correspondence between near-coastal El Niño events in the traditional sense (Quinn and Neal, 1992) and the basin-wide phenomenon that we are trying to monitor here. In this context, 'different flavors' of El Niño (Trenberth and Stepaniak, 2001; Kao and Yu, 2009) will be discussed in Section 5 of this paper.

It is noteworthy that the geographic migrations of our loading patterns with the seasonal cycle are not as pronounced in our analysis for 1871–2005 compared to 1950–2005, and even less than by doing the latter analysis for COADS (not shown here). It is possible that the pre-filtering through EOFs in reconstructed data reduces the excursions one would get from 'raw' COADS analyses back to 1871. However, COADS is not adjusted for observational biases (especially important for SST), and has poor coverage away from the major shipping lanes before the mid-20th century (e.g. Worley *et al*., 2005). Thus, we consider such pre-1950 COADS analyses to be unreliable. The spatial sense of the seasonal migrations in MEI.ext (Figure 2) is similar to the original COADS results in Wolter and Timlin (also Figure 2; 1993), even if smaller in range.

4.2. Basic temporal features of the MEI.ext

Figure 3 displays the time series of the MEI.ext (1871–2005) in three overlapping periods. High negative values of the MEI.ext represent the cold ENSO phase, a.k.a. La Niña, while high positive MEI.ext values represent the warm ENSO phase (El Niño). At the extremes, standardized departures above +2 have flagged the strongest El Niño events 8 times since 1871 (twice even above +3, in 1982–1983 and 1997–1998), with 4 such events since 1982, while only 5 of the strongest La Niña events have reached −2 standard deviations, with none since 1975–1976.

We computed means, standard deviations, and skewness coefficients for sliding 30-year periods (not shown here), and confirmed the well known reduction in ENSO activity levels from about 1920 through 1960, noted by Trenberth and Shea (1987) for the intensity of the SO. Owing to an apparent preference for La Niña events, the mean MEI.ext value for the early active period (before 1920) was negative, while the more recent active period (since 1960) averaged on the positive side, anchored by more El Niño events. The most extreme El Niño events (1877–1878, 1982–1983, and 1997–1998) occurred at the beginning and end of the 135-year record, explaining high positive skewness values during their respective 30-year periods. Some researchers have argued that ENSO behaviour underwent step-like changes around 1925, 1947, and 1977 (Hildago and Dracup, 2003). We looked at these specific periods as well, and can confirm that the MEI.ext values changed around these key

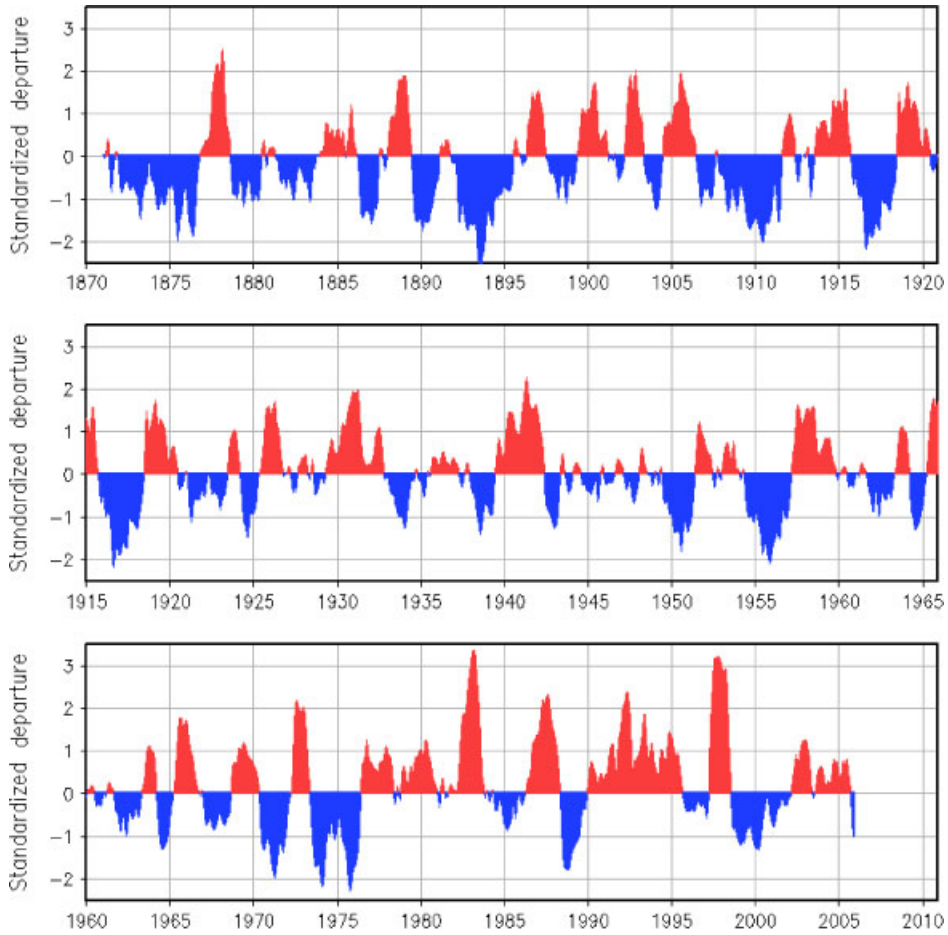

Figure 3. Time series of the MEI.ext. These plots follow the convention of the original MEI (http://www.esrl.noaa.gov/psd/people/klaus.wolter/MEI/), except that each seasonal value is normalized such that the mean value for 1871–2005 is '0' and the standard deviation is '1'. This figure is available in colour online at wileyonlinelibrary.com/journal/joc

dates, especially around 1976–1977 when their long-term average rose by more than 0.6 standard deviations for 1977–2005 compared to 1947–1976.

While every negative (positive) value of the extended MEI is flagged in blue (red), not every such value represents full-blown La Niña (El Niño) conditions. In fact, it is debatable as to what constitutes such an event. The current practice at CPC is to require at least *five running three-month seasons* to average above +0.5 °C (below −0.5 °C) for Niño 3.4 SST anomalies to be classified as an El Niño (La Niña) event (based on Kousky and Higgins, 2007). While this temperature threshold sets the bar fairly low, the CPC duration threshold removes short-lived events altogether, independent of their peak strength. For the period 1950–2005, CPC (http://www.cpc.noaa.gov/products/analysis_monitoring/ensostuff/ensoyears.shtml) flags 16 El Niño and 12 La Niña events, running in length from the required minimum of five running seasons up to 19 three-months seasons for the longest El Niño (1986–1988) and up to 37 three-month seasons for the longest La Niña (1973–1976). In the same CPC classification, the total number of cardinal (DJF, MAM, JJA, SON) seasons diagnosed as El Niño is 52 out of 224 possible, while 64 seasons are classified as La Niña. In other words, La Niña events often last longer than El Niño events, thus more than compensating for a smaller rate of occurrence. Because the 0.5 °C threshold is relatively easy to cross during the boreal autumn and winter seasons, about 60% of all cases are thus classified as either El Niño or La Niña, compared to around 40% for boreal spring and summer.

For comparison, Rasmusson (1984) generously counted 30 El Niño events from 1900 through 1979, or 37.5% of all years. He expanded his list based on the work of several historians such as Quinn (Quinn and Neal, 1992) who had listed a more modest 21 El Niño events in this timeframe. On the low end, Ropelewski and Halpert (1987) defined 18 El Niño years for the same 80-year period, but only allowed for the first year of El Niño to be counted.

Table II documents the rankings of four overlapping four-month seasons of the extended MEI: Nov–Feb, Feb–May, May–Aug, and Aug–Nov. We classify seasonal values to indicate strong/moderate/weak El Niño/La Niña, or neutral conditions, using percentile definitions: the top 10 percentiles at either end are considered **strong** (rank 13 and below for La Niña, rank 123 and above for El Niño), from the 10 percentile to the 20 percentile as **moderate**, and from the 20 percentile to the 30 percentile as **weak**; neutral conditions are assigned to all

ranks between the 30 and 70 percentiles (between ranks 42 and 94). The decade with the most frequent La Niña conditions of at least weak strength was the very first one on record: 24 out of 40 four-monthly seasons during 1871–1880 was far ahead of the first decade of the 20th century (18 cases) and the 1970s (17). While this appeared suspicious, we confirmed the unusual 1870s behavior by comparing the MEI.ext to Wright's (1989) CTI and SOI. El Niño conditions of at least weak strength were most common during the 1990s (23), followed by the 1910s with 18 such cases. Widening this comparison to include all possible sliding decades, 1986–1995 shows the most El Niño seasons, with 25 out of 40 possible cases, even more lop-sided than the highest ranked decade 1871–1880 with respect to La Niña. Near-neutral conditions (30–70 percentile) were most common during the 1940s (26), followed by the 1930s (22) and 1920s (21), confirming the general ENSO-weakness during the early- to mid-20th century.

Figure 4 illustrates the spacing of El Niño and La Niña events of at least moderate intensity (20 percentile threshold) for their bimonthly peak in the MEI.ext record. Here, 'spacing' is defined as the length of time between the onset of the preceding ENSO event and the onset of the current event of the same sign. 'Onset' refers to the first bimonthly season that reaches the 30 percentile threshold (ranked at or below 41st for La Niña, and at or above 95th for El Niño). In Figure 4(a), the first (left) symbol in the El Niño panel refers to the 1885 event that reached the 30 percentile threshold in August–September of that year, 8 years and 3 months after the previous El Niño had started in May–June of 1877. The last (right) symbol in the La Niña panel (Figure 4(b)) refers to an event that started in September–October of 2005, and lasted past the end of 2005. Within the 135-year MEI.ext record, there are 33 El Niño and 30 La Niña events defined in this manner, or 32 (29) El Niño (La Niña) spacings. This tally is higher than one would infer from Table II, which is based on 4 out of 12 possible overlapping 4-month seasons, thus letting short-lived events 'fall through the cracks'.

El Niño events have shown a clear preference to occur every 2–5 years (21 of 32 event spacings fall into this category), with a slight downward trend in spacing (or periodicity) over the period of record (Figure 4(a)). This is mostly due to the absence of long El Niño-free periods since 1951: there were 5 El Niño events more than 6 years apart from others before then, but none since. An upward trend in the spacing of La Niña events (Figure 4(b)) appears to be more prominent, explaining over 30% of the variance since 1871. In fact, the last three La Niña events of this record (starting in 1988, 1998, and 2005) were 7–15 years apart from each other and the previous long-lived La Niña that started in 1973. However, since a new La Niña event began just two years after 2005, and again in 2010, the upward trend in La Niña spacings has at least been interrupted. Overall, La Niña events have shown a broader spectrum than El Niño events, being up to 15 years apart (*vs* up to 11 years for

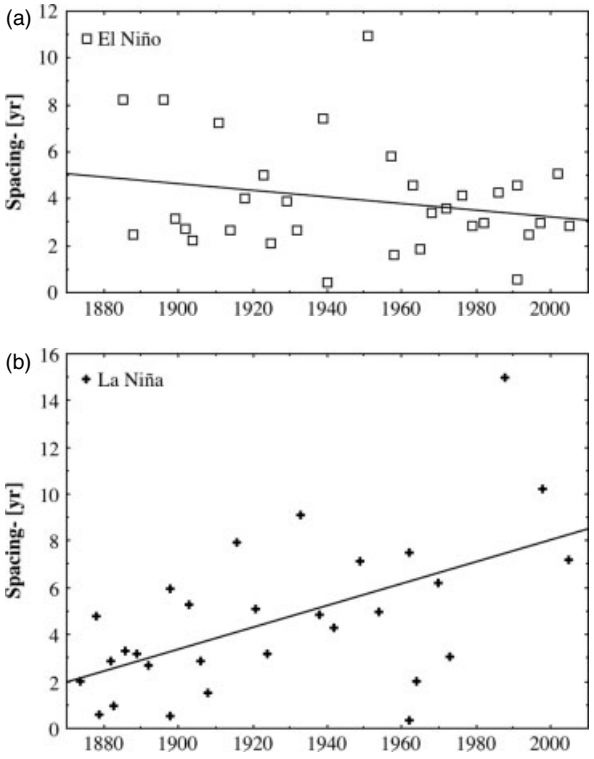

Figure 4. (a) Spacing of El Niño (top; r**2 = 5.0%) events through the full period of record, based on MEI.ext. Spacing is given in years between onsets of events. (b) Spacing of La Niña (bottom; r**2 = 31.6%) events through the full period of record, based on MEI.ext. Spacing is given in years between onsets of events.

El Niño), and are less likely to fall into the most common 2–5-year spectral band (11 of 29 cases).

This paper does not document the behaviour of individual strong El Niño and La Niña events in comparison figures analogous to the ones we have posted on the original MEI website (http://www.noaa.esrl.noaa.gov/psd/people/klaus.wolter/MEI/). However, a parallel 'MEI_ext' website with such figures will be created (and linked to the original MEI website) to accompany this publication. This website will also enable users to download the full MEI.ext time series.

4.3. Lagged features in MEI.ext

Figure 5 shows the 2-month persistence of bimonthly MEI.ext values. This was computed for 5 non-overlapping 30-year periods: 1886–1915, 1916–1945, 1946–1975, and 1976–2005. There appear to be subtle shifts of the boreal spring *minimum* that used to centre on the April–May to June–July, or May–June to July–August transitions (in the earliest two 30-year periods), then dropped back about 1 month in the 30-year period immediately after WW II, only to return to the prior timing of this minimum in the most recent 30-year period (Figure 5). In other words, the boreal 'spring-persistence-barrier' (McPhaden, 2003) has remained an essential feature of the ENSO phenomenon through more than a century of recorded history. On the other hand, peak persistence used to be recorded in the boreal autumn season (highest values from September–October

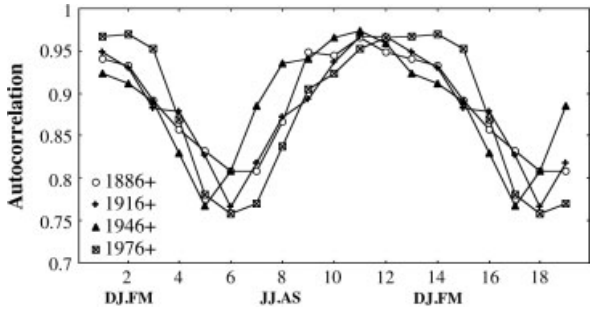

Figure 5. Two-month lag correlations of the MEI.ext as a function of the seasonal cycle ('2' and '14' refer to lag correlations from Dec–Jan to Feb–Mar, etc.). The four line graphs refer to the periods 1886–1915, 1916–1945, 1946–1975, and 1976–2005.

to November–December were common in the first three 30-year periods), while it has shifted to boreal winter in the most recent 30-year epoch (December–January to February–March; Figure 5).

The remainder of this subsection explores the interplay among duration of ENSO events, their peak amplitudes, and their spacing. We use the definition of ENSO events given in the previous subsection, requiring at least one bimonthly season to reach the 20 percentile threshold (moderate intensity) in either tail to qualify as an event. 'Duration' is the temporal difference between the first (onset) bimonthly season of an ENSO event to reach the 30 percentile threshold and the last (demise) bimonthly season to do so. To accommodate minor intraseasonal fluctuations, we allow for bimonthly ranks to drop into the neutral range (30–70 percentile) for 1 month only, but not for 2 months in a row. Despite the differences in temporal behavior noted in Section 4.2, both El Niño and La Niña events share a *median* duration of 13 months in the MEI.ext record. The *average* duration of La Niña events is 2 months longer than that of El Niño events: 15.5 *versus* 13.5 months, reflecting the fact that the 5 longest-lived La Niña events outlasted any El Niño (Figure 6).

Figure 6 documents the relationship between peak amplitude and duration for both El Niño and La Niña events. Focusing first on El Niño events (Figure 6(a)), the size of its peak amplitude is clearly associated with its duration, in the sense that long-lived events typically show higher peak values than short-lived events. This linear association explains just over one third of the total variance of either variable. However, the 3 highest El Niño peaks occurred during events that lasted 'only' between 1 and 1.5 years (1877–1878, 1982–1983, and 1997–1998), just above the median length of El Niño events. Nevertheless, it makes physical sense that El Niño events that reach larger amplitudes take longer to build as well as to dissipate, so this result is not unexpected. There were two such events that lasted longer than 2 years: starting in 1940 and 1991, both stayed above the 30 percentile level for exactly 28 months. In the MEI.ext framework, the long-lived El Niño of the early 1990s was just as long as its lesser-known cousin of the early 1940s.

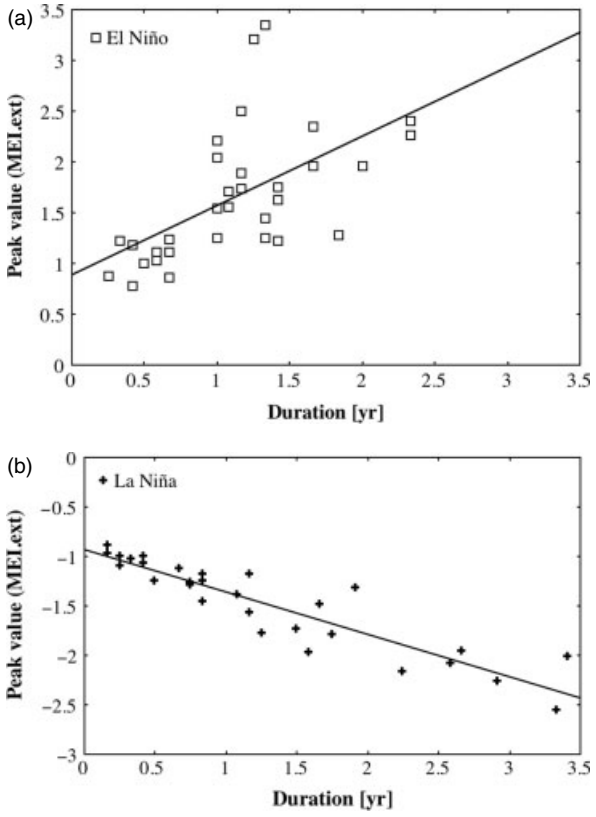

Figure 6. (a) Peak amplitudes for MEI.ext of El Niño (top; r**2 = 33.5%) events as a function of the duration of these events, defined as the length of time that each event of at least moderate (20 percenttile) peak intensity stays above the 30 percentile threshold, allowing for one-month 'slip-ups'. (b) Peak amplitudes for MEI.ext of La Niña (bottom; r**2 = 83.5%) events as a function of the duration of these events, defined as the length of time that each event of at least moderate (20 percentile) peak intensity stays above the 30 percentile threshold, allowing for one-month 'slip-ups'.

This is noteworthy since the more recent El Niño has been used as evidence for anthropogenic climate change, also arguing that the recurrence interval of such a long-lived event could be well over 1000 years (Trenberth and Hoar, 1997). To be fair, Trenberth and Hoar, using Darwin SLP and Niño 3.4 SST, had looked at runs above the *median* of all values (50 percentile), the lowest possible threshold for El Niño events. In that spirit, the period from November–December 1989 through July–August 1995 was indeed the longest on record to stay continuously above the median for the MEI.ext (69 months), far ahead of its nearest competitors: April–May 1929 through September–October 1932 (42 months), and May–June 1939 through April–May 1942 (36 months).

Turning our attention to La Niña (Figure 6(b)), we diagnose exceptional coupling between duration and amplitude of the cold phase of the ENSO cycle: 83.5% explained variance is just about as tight a relationship as can be found in observational records. If we break down the duration of a La Niña event into a ramp-up phase from onset to its peak, and a dissipation phase from its peak to its demise, the linear relationships between peak values and ramp-up as well as dissipation times are

very strong for both, at 54 and 66% explained variance, respectively (not shown here). In fact, it takes just about as long to grow a large La Niña event as it takes to bring it to its end. As mentioned before, it is also apparent that La Niña events can last longer than El Niño, with five events surviving more than 2.5 years, longer than any El Niño by this measure, reaching 41 months for the 1908–1911 event, and 40 months for the 1892–1895 La Niña. On the other hand, the two shortest, 'aborted' La Niña events lasted only two sliding bimonthly seasons each (both in 1962), attesting to a wider range of duration for La Niña events than El Niño. It is beyond the scope of this paper to discuss the complicated reasons that determine the duration of ENSO events, but the reader is referred to Eccles and Tziperman (2004), Kleeman (2008), and MacMynowski and Tziperman (2008) that explore both linear and nonlinear mechanisms for this at length. Returning to the issue of the longest-lasting La Niña events in the sense of Trenberth and Hoar (1997), it is perhaps noteworthy that one of the three longest-lasting runs *below* the MEI.ext median was completed just in this millennium (1998–2002: 43 months), while the other two occurred about a century ago: 1891–1895 (45 months), and 1907–1911 (46 months). However, all three of these La Niña-like conditions ended considerably sooner than the El Niño-like run of late 1989 into 1995.

Figure 7 illustrates perhaps the most interesting relationship documented in this paper, between the spacing of El Niño events and the peak amplitude reached, for the recent (post-1950) and 'old' (1871–1949) record. We are focusing on El Niño events here since we did not find an analogous relationship for La Niña events. For the early part of the record (pre-1950), there is a strong tendency for the peak value of the MEI.ext to be higher for shorter periodicities than for longer ones, explaining 48% of the variance of this 15 case sample. Since 1950, this relationship has been much weaker (4.7% explained variance), but with similar regression parameters. One remarkable aspect about this is that the duration of ENSO events tends to be positively correlated with the spacing of ENSO events (not shown). Hence, longer periodicities of ENSO events tend to be associated with longer duration events. Comparing Fig. 7 with Figure 6(a), the findings of longer duration El Niño events being associated with higher amplitude peaks *versus* higher El Niño peaks paired with shorter periodicities appear contradictory. However, the spacing *versus* peak relationship (Figure 6(a)) refers to the spacing between the onset of the *previous* El Niño and the *current* one, while the duration *versus* peak relationship (Figure 7) refers to the duration of the current El Niño. Since shorter El Niño events tend to alternate with longer ones (not shown here), we can have a short spacing interval followed by a long-lived and high-peak El Niño that would be entirely consistent with both Figures 6(a) and 7.

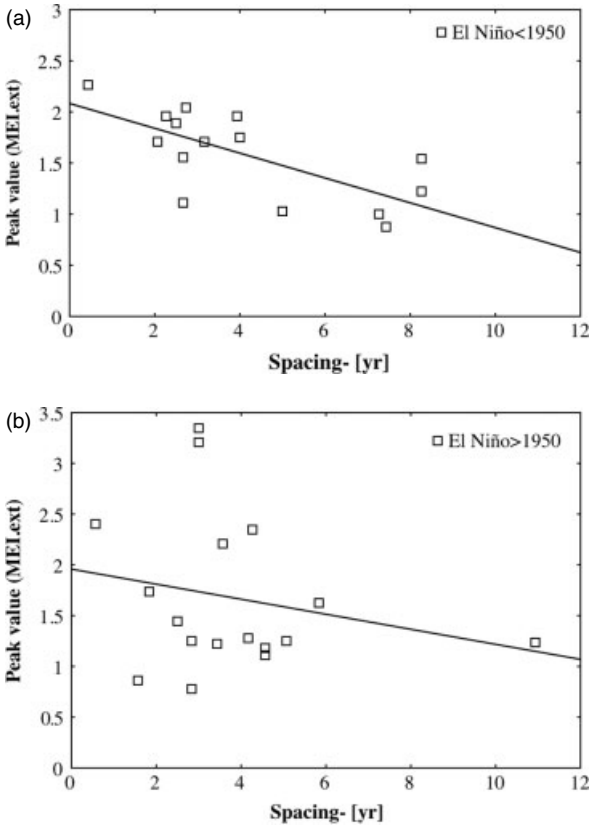

Figure 7. (a) Peak amplitudes of El Niño events based on the MEI.ext before 1950 (top; r**2 = 48.0%) as a function of the spacing from onset to onset of these events. (b) Peak amplitudes of El Niño events based on the MEI.ext after 1950 (bottom; r**2 = 4.7%) as a function of the spacing from onset to onset of these events.

5. Discussion and concluding remarks

In the context of monitoring and diagnosing ENSO activity, there are three reasons we find the MEI (and MEI.ext) approach compelling:

1. ENSO is, by its very nature, a multivariate phenomenon, coupling the tropical Pacific to the overlying atmosphere in several ways, so an index that reflects these multiple characteristics rather than just the main one from one variable field (e.g. SOI, Niño 3.4 SST) appears to be a more balanced and complete way to monitor the ENSO state;
2. The MEI has less vulnerability to errors than single station (or even single variable) fields; problems with Tahiti station data have long plagued the SOI (e.g. Allan *et al*., 1991), and Niño 3.4 SST was very poorly sampled prior to the late 1950s, achieving high-quality measurements only during the satellite era and with the installation of the TOGA-TAO array in the 1980s;
3. While researchers have commented on seasonal dependencies of the ENSO cycle (Rasmusson and Carpenter, 1982; Philander, 1990), both the SOI and Niño SST regions are spatially fixed throughout the year. The MEI is the only ENSO index that allows for spatial variations of its key features with the seasonal cycle, even though this characteristic is somewhat muted for

the MEI.ext, and by definition represents a weighted average of all its features.

This paper describes our first extended Multivariate ENSO Index (MEI.ext) that covers almost the full historical record (1871–2005). By focusing on the most fundamental portions of the original MEI, the SLP and SST fields, we have computed a 'minimalist' version of the MEI from reconstructed Hadley Centre data that appears to capture ENSO behaviour since the late 19th century reasonably well.

Despite its distinguishing characteristics, the MEI.ext correlates highly with other ENSO indices, so there is no question that they all monitor the same phenomenon in boreal winter. Differences are most noticeable in boreal summer, so that the choice of the ENSO index may influence the results one can get from using it for, say, ENSO impacts research. In the context of anthropogenic climate change, it is of paramount importance to have the most reliable ENSO index for the longest possible record in order to be able to differentiate between 'natural' and anthropogenically altered climate variability associated with ENSO. The MEI.ext offers a robust multivariate alternative to a handful of existing ENSO indices that cover the instrumental record back to the late 19th century.

For the period of record that we investigated (1871–2005), the MEI.ext shows that many features of recent ENSO variability are not quite as unusual as sometimes claimed. The overall ENSO activity level of recent decades is comparable to the situation about a century ago, while the early- to mid-20th-century 'slump' in activity was the odd portion of the record. In terms of event spacing, the dearth of La Niña events from 1976 to 2005 is one of the features that stands out in the 135-year record, but appears to have been superseded by more active La Niña behaviour since then. The long duration of the early 1990s El Niño event is comparable to that of the early 1940s. Only by relaxing the El Niño threshold from the upper 30 percentile to the median does the early 1990s period appear as excessive as Trenberth and Hoar (1997) asserted. Independent of the threshold used, long-lived La Niña events have occurred through the full record. The boreal spring-persistence-barrier appears to be a fundamental and recurrent feature of ENSO through the sampled instrumental record. It goes along with a preference for event onsets in boreal spring and summer that has never been quite as phase-locked to the seasonal cycle as suggested by, e.g. Philander (1990), but has remained essentially unchanged since 1871. We propose that a good fraction of the more pronounced lack of persistence of conventional ENSO indices compared to the MEI and MEI.ext during boreal spring is due to their inability to monitor typical spatial migrations of key ENSO features during that time of year.

This paper documents a linear relationship between peak amplitude and duration of ENSO events, in particular during the La Niña phase. This may be useful for predictive purposes. On the other hand, we found an inverse dependency of the peak amplitude of El Niño events on periodicity or spacing (higher El Niño peaks during more frequent events). Eccles and Tziperman (2004) have argued that nonlinear feedback mechanisms may be responsible for exactly this type of relationship, and An and Jin (2004) give independent arguments for the nonlinear nature of El Niño events, but it is beyond the scope of this paper to address this issue more deeply.

The MEI cannot differentiate between 'different flavours' of El Niño (Trenberth and Stepaniak, 2001), or weigh in on the debate whether there are fundamentally different so-called Eastern-Pacific *versus* Central-Pacific events (Kao and Yu, 2009). It was ironic to witness the very first El Niño after Rasmusson and Carpenter (1982) described the 'canonical sequence' of El Niño events as a *westward* propagating phenomenon from the eastern Pacific, to be the 1982–1983 'Super-El Niño' that propagated *eastward* from the Central Pacific. There were several more events of this type since then, most prominently the 1986–1988 and 1991–1995 events, leading some to proclaim that there had been a fundamental shift in behaviour (Trenberth and Stepaniak, 2001). For the newer record, we can confirm that central Pacific events tend to start later in the calendar year than eastern-Pacific events (Kao and Yu, 2009), but found that most events of either type end up becoming basin-wide nevertheless, rendering their distinction less meaningful once fully established. In a related matter, we understand that so-called El Niño Modoki events (Weng *et al*., 2007, 2009) are simplified versions of the 2nd principal component of the tropical Pacific SST field which by definition is orthogonal to the 1st principal component of this field (which, in turn, depicts the SST pattern associated with ENSO). However, since the Modoki SST pattern is frozen in space through the year (Weng *et al*., 2007), while the MEI (and MEI.ext) shows some seasonal variation of its loading patterns, it turns out that the MEI is not always orthogonal to Modoki SST. In fact, from April–May to June–July, the MEI.ext time series correlates with the Modoki time series around −0.35 between 1950 and 2005. During this time of year, the existence of an El Niño Modoki event would thus be more consistent with La Niña than with El Niño, as monitored by the MEI.ext.

Going back in time, it is questionable whether reconstructed SST data can be used to reliably differentiate between different types of ENSO events back into the 19th century. For *some* stronger events (e.g. 1896–1897 and 1902–1903), we can diagnose onset HadSST El Niño anomalies in the central Pacific rather than eastern Pacific well before the 1976 'switch' that has been associated with several such events in a row (Trenberth and Stepaniak; 2001, Kao and Yu, 2009; and Sun and Yu, 2009). Since the MEI.ext SST loadings are high for much of the equatorial cold tongue, we believe that both types of ENSO events project reasonably well on the MEI, reducing the risk of letting any event slip by even if it were to remain confined to the eastern or western portion of that region.

Variations in ENSO activity on decadal and longer time scales warrant further research. While there have been claims that the 'Pacific Decadal Oscillation' may play a large role in this (Hidalgo and Dracup, 2003), there is sufficient intrinsic variability in the tropical Pacific system (MacMynowski and Tziperman, 2008; Sun and Yu, 2009) to not require extratropical forcing to accomplish this.

One final caveat: Weak ENSO events were mostly ignored in this paper in which we required at least one bimonthly peak value to cross the moderate (20 percntile) threshold to be considered for most of the analysis. Such weak events tend to come and go faster than their moderate and strong cousins, often hovering right around the weak (30 percnetile) threshold. In fact, there are some even weaker and debatable 'ENSO events' (e.g. the 'La Niña' of 1995–1996 and the 'El Niño' of early 1990) that never even reach the 30 percentile threshold for the MEI.ext (Table II). Of course, thresholds for weak (moderate, or strong) ENSO events are somewhat arbitrary – we decided to put the same number of seasons in each category, and keep the percentage of near-neutral ENSO conditions as the biggest category (40%). Using the ranked and numerical MEI.ext values (to be posted on the new MEI_ext website), interested parties should be able to come up with their own categorisations if so desired.

The MEI.ext was not created nor do we intend to replace the MEI with it for present-day monitoring of ENSO. In fact, we have been testing a variety of alternative versions of the present-day MEI that aim to exploit the observational and modelling advances that have occurred in the last three decades. This will be reported elsewhere.

Acknowledgements

We wish to express our gratitude to the organizers of CLIMAR-III for a wonderful conference in 2008. Funding for this activity was provided by the US National Weather Service Climate Services branch. Within that agency, we thank Fiona Horsfall for her support and feedback. We are also very grateful to Tony Barnston (IRI) for his thorough manuscript review that helped to improve our paper in many different ways. Any opinions, findings, conclusions, or recommendations are those of the authors and do not necessarily reflect the views of the Illinois State Water Survey or the funding agency.

References

Allan RJ. 2000. ENSO and climate variability in the past 150 years. In *El Niño and the Southern Oscillation: Multiscale Variability and global and regional impacts*, Diaz HF, Markgraf V (eds). Cambridge University Press: Cambridge; pp. 3–55.

Allan RJ, Ansell T. 2006. A new globally complete monthly historical gridded mean sea level pressure dataset (HadSLP2): 1850–2004. *Journal of Climate* **19**: 5816–5842.

Allan RJ, Nicholls N, Jones PD, Butterworth IJ. 1991. A further extension of the Tahiti-Darwin SOI, early SOI results and Darwin pressure. *Journal of Climate* **4**: 743–749.

An SI, Jin FF. 2004. Nonlinearity and asymmetry of ENSO. *Journal of Climate* **17**: 2399–2412.

Bjerknes J. 1966. A possible response of the atmospheric Hadley circulation to equatorial anomalies of ocean temperature. *Tellus* **18**: 820–829.

Barnston AG, Chelliah M, Goldenberg SB. 1997. Documentation of a highly ENSO-related SST region in the Equatorial Pacific. *Atmosphere-Ocean* **35**: 367–383.

Bjerknes J. 1969. Atmospheric teleconnections from the equatorial Pacific. *Monthly Weather Review* **97**: 163–172.

Eccles F, Tziperman E. 2004. Nonlinear effects on ENSO's period. *Journal of Atmospheric Sciences* **61**: 474–482.

Hidalgo HG, Dracup JA. 2003. ENSO and PDO effects on hydroclimatic variations of the Upper Colorado River Basin. *Journal of Hydrometeorology* **4**: 5–23.

Kao HY, Yu JY. 2009. Contrasting Eastern-Pacific and Central-Pacific types of ENSO. *Journal of Climate* **22**: 615–632.

Kaplan A, Cane MA, Kushnir Y, Clement AC, Blumenthal MB, Rajagopalan B. 1998. Analyses of global sea surface temperature 1856–1991. *Journal of Geophysical Research* **103**: 18567–18589.

Kleeman R. 2008. Stochastic theories for the irregularity of ENSO. *Philosphical transactions of the Royal Society A* **366**: 2511–2526, DOI:10.1098/rsta.2008.0048.

Kousky VE, Higgins RW. 2007. An alert classification system for monitoring and assessing the ENSO cycle. *Weather and Forecasting* **22**: 353–371.

Lorenz EN. 1956. Empirical orthogonal functions and statistical weather prediction. Scientific Report No. 1. Department of Meteorology, MIT (NTIS AD 110268).

MacMynowski DG, Tziperman E. 2008. Factors affecting ENSO's period. *Journal of Atmospheric Sciences* **65**: 1570–1586.

McPhaden MJ. 2003. Tropical Pacific Ocean heat content variations and ENSO persistence barriers. *Geophysical Research Letters* **30**: 1480, DOI:10.1029/2003GL016872.

Philander SG. 1990. *El Niño, La Niña, and the Southern Oscillation*. Academic Press: San Diego.

Quinn WH, Neal VT. 1992. The historical record of El Niño events. In *Climate since A.D. 1500*, Bradley RS, Jones PD (eds). Routledge: London; 623–648.

Ramage CS. 1987. Secular change in reported surface wind speeds over the ocean. *Journal of Applied Meteorology* **26**: 525–528.

Rasmusson EM. 1984. El Niño: The ocean/atmosphere connection. *Oceanus* **27**: 5–12.

Rasmusson EM, Carpenter TH. 1982. Variations in tropical sea surface temperatures and surface wind fields associated with the Southern Oscillation/El Niño. *Monthly Weather Review* **110**: 354–384.

Rayner NA, Brohan P, Parker DE, Folland CK, Kennedy JJ, Vanicek M, Ansell TJ, Tett SFB. 2006. Improved analyses of changes and uncertainties in sea surface temperature measured in situ since the mid-nineteenth century: The HadSST2 dataset. *Journal of Climate* **19**: 446–469.

Rayner NA, Parker DE, Horton EB, Folland CK, Alexander LV, Rowell DP. 2003. Global analyses of sea surface temperature, sea ice, and night marine air temperature since the late nineteenth century. *Journal of Geophysical Research* **108**(D14): 4407, DOI:10.1029/2002JD002670.

Ropelewski CF, Halpert MS. 1987. Global and regional scale precipitation patterns associated with the El Nino/Southern Oscillation. *Monthly Weather Review* **115**: 1606–1626.

Smith CA, Sardeshmukh P. 2000. The Effect of ENSO on the Intraseasonal Variance of Surface Temperature in Winter. *International Journal of Climatology* **20**: 1543–1557.

Smith TM, Reynolds RW. 2003. Extended reconstruction of global sea surface temperatures based on COADS data (1854–1997). *Journal of Climate* **16**: 1495–1510.

Smith TM, Reynolds RW. 2004. Improved extended reconstruction of SST (1854–1997). *Journal of Climate* **17**: 2466–2477.

Sun F, Yu JY. 2009. A 10-15-Yr modulation cycle of ENSO intensity. *Journal of Climate* **22**: 1718–1735.

Trenberth KE, Hoar TJ. 1997. El Niño and climate change. *Geophysical Research Letters* **24**: 3057–3060.

Trenberth KE, Shea DJ. 1987. On the evolution of the Southern Oscillation. *Monthly Weather Review* **115**: 3078–3096.

Trenberth KE, Stepaniak DP. 2001. Indices of El Niño evolution. *Journal of Climate* **14**: 1697–1701.

Troup AJ, 1965. The Southern Oscillation. *Quarterly Journal of the Royal Meteorological Society* **91**: 490–506.

Walker GT, Bliss EW. 1932. World weather V. *Memoirs of the Royal Meteorological Society* **4**: 53–84.

Weng H, Ashok K, Behera S, Rao SA, Yamagata T. 2007. Impacts of recent El Niño Modoki on dry/wet conditions in the Pacific rim during boreal summer. *Climate Dynamics* **29**: 113–129.

Weng H, Behera S, Yamagata T. 2009. Anomalous winter climate conditions in the Pacific rim during recent El Niño Modoki and El Niño events. *Climate Dynamics* **32**: 663–674.

Wolter K. 1989. Modes of tropical circulation, Southern Oscillation, and Sahel rainfall anomalies. *Journal of Climate* **2**: 149–172.

Wolter K, Timlin MS. 1993. Monitoring ENSO in COADS with a seasonally adjusted principal component index. *Proceedings of the 17th Climate Diagnostics Workshop*, Norman, OK, NOAA/NMC/CAC, NSSL, Oklahoma Climate Survey, CIMMS and the School of Meteorology, University of Oklahoma: Norman, OK; 52–57.

Wolter K, Timlin MS. 1998. Measuring the strength of ENSO events – how does 1997/98 rank? *Weather* **53**: 315–324.

Worley SJ, Woodruff SD, Reynolds RW, Lubker SJ, Lott N. 2005. ICOADS Release 2.1 data and products. *International Journal of Climatology (CLIMAR-II Special Issue)* **25**: 823–842, DOI:10.1002/joc.1166.

Wright PB. 1975. *An index of the Southern Oscillation*. University of East Anglia, Climate Research Unit, CRU RP4.

Wright PB. 1984. Relationships between indices of the Southern Oscillation. *Monthly Weather Review* **112**: 1913–1919.

Wright PB. 1989. Homogenized long-period Southern Oscillation indices. *International Journal of Climatology* **9**: 33–54.

